Recd 12 Jan 89
C.W. Litton

(2)

SECURITY CLASSIFICATION OF THIS PAGE

DOCUMENTATION PAGE

Form Approved
OMB No. 0704-0188

AD-A205 058

DTIC ELECTE JAN 16 1989 S D CS

1b. RESTRICTIVE MARKINGS

DTIC FILE COPY

3. DISTRIBUTION/AVAILABILITY OF REPORT
Approved for public release; distribution unlimited.

4. PERFORMING ORGANIZATION REPORT NUMBER(S)
CLS-88-102

5. MONITORING ORGANIZATION REPORT NUMBER(S)
AFOSR-TR- 89-0082

6a. NAME OF PERFORMING ORGANIZATION	6b. OFFICE SYMBOL (If applicable)	7a. NAME OF MONITORING ORGANIZATION
University of Southern California		AFOSR

6c. ADDRESS (City, State, and ZIP Code)
Center for Laser Studies
Los Angeles, CA 90089-1112

7b. ADDRESS (City, State, and ZIP Code)
BLG 410
BAFB DC 20332-

8a. NAME OF FUNDING/SPONSORING ORGANIZATION	8b. OFFICE SYMBOL (If applicable)	9. PROCUREMENT INSTRUMENT IDENTIFICATION NUMBER
AFOSR	NE	AFOSR-88-0038

8c. ADDRESS (City, State, and ZIP Code)
BLG 410
Bolling Air Force Base, DC 20332

10. SOURCE OF FUNDING NUMBERS

PROGRAM ELEMENT NO.	PROJECT NO.	TASK NO.	WORK UNIT ACCESSION NO.
61102F	2306	B1	

11. TITLE (Include Security Classification)
Thermal Transport Studies of Optical Coatings, Interfaces, and Surfaces by Thermal Diffusion Wave Interferometry

12. PERSONAL AUTHOR(S)
Randall T. Swimm

13a. TYPE OF REPORT	13b. TIME COVERED	14. DATE OF REPORT (Year, Month, Day)	15. PAGE COUNT
Annual Technical	FROM 12/1/87 TO 11/30/88	1989, Jan. 9	24

16. SUPPLEMENTARY NOTATION

17. COSATI CODES			18. SUBJECT TERMS (Continue on reverse if necessary and identify by block number)
FIELD	GROUP	SUB-GROUP	Optical Coatings, Thermal Transport. (mgm)

19. ABSTRACT (Continue on reverse if necessary and identify by block number)

An improved measurement system for performing thermal transport studies in coatings, interfaces, and surfaces has been developed and implemented. A major source of systematic error in earlier work has been discovered and eliminated. Measured data are in qualitative agreement with theoretically predicted behavior; numerical fitting of the data constitutes the next research phase. Efforts continue to characterize in detail thermal transport in simple, thin layered structures. Initial theoretical modelling of more complicated two-layer structures is reported.

(1)

UNCLASSIFIED

20. DISTRIBUTION/AVAILABILITY OF ABSTRACT
☐ UNCLASSIFIED/UNLIMITED ☐ SAME AS RPT. ☐ DTIC USERS

21. ABSTRACT SECURITY CLASSIFICATION

22a. NAME OF RESPONSIBLE INDIVIDUAL	22b. TELEPHONE (Include Area Code)	22c. OFFICE SYMBOL
DR LITTON	(202) 767-4931	NE

DD Form 1473, JUN 86 Previous editions are obsolete. SECURITY CLASSIFICATION OF THIS PAGE

Report CLS-88-102

THERMAL TRANSPORT STUDIES OF OPTICAL COATINGS, INTERFACES AND SURFACES BY THERMAL DIFFUSION WAVE INTERFEROMETRY

Randall T. Swimm, Principal Investigator
Center for Laser Studies
University of Southern California
Los Angeles, CA 90089-1112

9 January 1989

Annual Technical Report

Contract Number AFOSR-88-0038

Prepared for
Air Force Office of Scientific Research
Bolling Air Force Base, DC 20332

TABLE OF CONTENTS

TABLE OF FIGURES

2.0 TECHNICAL DISCUSSION

2.1 BACKGROUND

2.1.1 Background Summary

The basic system operation is explained in Ref. 6. A brief summary of the system operation is as follows. Consider a sample consisting of a single-layer thin metal coating deposited on a transparent dielectric substrate. The objective is to measure the thermal transport properties of the coating/substrate system. The method of measurement is a new technique called diffusion-wave interferometry. The measurement involves two steps: sinusoidal heating of the metal coating surface, and measurement of the sinusoidal temperature response of the metal coating surface.

2.1.2 Theoretical Background

Under one-dimensional operating conditions, the sinusoidal heating generates a critically-damped steady state temperature field known as a thermal diffusion wave:

$$T(x,t) = T_o\, e^{-kx} \cos(kx - \omega t + \phi)$$

where T is temperature, k is wavenumber, ω is angular frequency, x is distance and t is time (ref. 6). Because the thermal-diffusion wave is partially reflected at the coating-substrate interface, the sinusoidal temperature response

at the metal coating surface is out of phase with the sinusoidal heating. Changing the modulation frequency of the heating causes the wave number k of the thermal diffusion wave to change. Measurement of the phase shift between the heating and the temperature response as a function of the modulation frequency yields an interference oscillation in the phase that allows the thermal transport properties of the coating/substrate system to be determined.

2.1.3 Experimental Background

The sinusoidal heating is produced using an argon-ion pump laser whose intensity is modulated by an electrooptic modulator. The temperature response is measured by reflecting an unmodulated HeNe laser beam off the sample, and measuring the intensity modulation induced by sinusoidal modulation of the metal coating reflectivity (caused by the temperature dependence of the metal coating reflectivity). The reflected HeNe beam is monitored using a photoconductive detector, and a lock-in analyzer is used to measure the resulting weak synchronous signals.

2.2 SYSTEM UPGRADE

2.2.1 Pump Laser

The original system included a 100 mW argon-ion pump laser. This laser was adequate for the initial studies. However, the low power required that a fairly small spot diameter be used in order

to obtain sufficient heating to yield an acceptable signal to noise ratio. For simplicity of data analysis, it is desirable that radial heat flow be negligible at all modulation frequencies employed. This one-dimensional operating requirement is equivalent to requiring that the thermal diffusion length be much less than the pump spot radius at all modulation frequencies employed. Therefore, the lowest operating frequency within the one-dimensional limit is limited by the spot diameter used. In order to increase the system dynamic range over which the modulation frequency may be varied within one-dimensional operation, the 100 mW pump laser was replaced by 6W argon-ion laser. As will be shown later, attaining the greatest possible dynamic range is the key to assuring uniqueness of parameter fit when analyzing the data.

2.2.2 Electrooptic Modulator

An electrooptic modulator is used to modulate the intensity of the pump laser beam. Although the original electrooptic modulator was specified to operate at laser powers up to 10W, it was found that modulated beam quality was unacceptable above 100 mW of pump power, apparently due to thermal lensing in the index matching fluid. A custom-designed electrooptic modulator with reduced optical path length within the index matching fluid was obtained under warranty from the modulator manufacturer.

2.2.3 Signal Detector

A photoconductive detector is used to detect the weak intensity modulation induced on the probe HeNe beam. The detector housing originally in use failed to provide adequate shielding at frequencies above 10 kHz. The temporary solution to this problem was to measure the synchronous background, and subtract it from the signal plus background. This subtraction resulted in a reduction of the signal to noise ratio by a factor of about 2. An improved detector housing was installed, reducing the synchronous background to a negligible level.

2.2.4 Rear-surface Probe

The system configuration at the start of the contract allowed the temperature modulation of the film/air interface to be monitored using a HeNe laser relying on the temperature modulation of the metal coating reflectivity. An additional probe layout has been installed to allow temperature modulation measurements at the film/substrate interface for metal coatings deposited on a transparent substrate (See Ref. 5 for a similar technique). In this case, a HeNe laser beam passes through the substrate to strike the metal coating at a point centered within the region heated by the pump laser beam. After being reflected by the metal coating, the rear HeNe probe beam exits through the substrate, and after passing through a relay lens enters a photoconductive detector identical to that used to monitor the front-surface probe beam. The relay lens is needed to form an

imaging system. Without the relay lens, probe beam deflection introduced by a pump-induced thermal lens in the substrate would otherwise give rise to a strong synchronous signal due to detector reponse inhomogeneity. Data from the rear-surface probe provides at least one independent condition when fitting adjustable parameters during data anlysis. This addtional independent data correspondingly reduces the necessary system dynamic range required to insure uniqueness of parameter fit.

2.3 SYSTEMATIC ERROR

2.3.1 Details

A major systematic error has been discovered and eliminated. The error entered during the calibration of system electronic phase shift. As discussed in section 2.1, the phase shift between the sinusoidal heating of the metal coating surface and the sinusoidal temperature response of the metal coating surface constitutes the desired data. The lock-in analyzer provides a phase shift value, but this value includes electronic phase shift introduced in the detector and preamplifier. In order to calibrate this electronic phase shift, the pump beam is directed into the probe detector. A nonzero phase shift is assumed to be electronic in origin. However, an error occurred due to the presence of a red colored glass filter. This filter passes HeNe laser light, but absorbs argon laser light. The filter is used to eliminate scattered pump light during probe beam measurements.

However, during calibration of the electronic phase shift, the pump beam was originally directed through the glass filter into the probe detector. Precautions were taken to reduce the intensity of the pump light sufficiently to reduce heating in the glass filter to a (hopefully) negligible level. The criterion used was that the measured phase be independent of the pump power over a two decade range of pump power. Unfortunately, this criterion proved to be inadequate, and a large difference in phase was found to occur between calibration readings taken with and without the glass filter.

2.3.2 Implications

The discovery of a major systematic error after two years of operation serves to illustrate the need for a wide dynamic range of modulation frequency and consequently of thermal diffusion-wave length. Had this error not been discovered by accident, a problem would have been ultimately encountered in fitting the data over the newly-increased dynamic range. However, it would not have been clear whether the problem was due to the presence of a systematic error, or to the inadequacy of the sample model, say due to supposed coating inhomogeneity. Many such sizeable systematic errors have already been discovered and eliminated. More such errors may still be present. Measurements will continue on the simplest possible samples (i.e. single metal layers, or solid metal mirrors) until there is good cause to believe that the measurements are free of non-negligible

systematic errors.

2.4 RESULTS

2.4.1 Description of Figures

Data have been measured on a 1000 Å Ni coating deposited on an SiO_2 substrate by e-beam deposition. The data are shown in Figs. 1 and 2, and representative theoretical model behavior is shown in Figs. 3 and 4, for comparison. (The theoretical plots are not the result of fitting the experimental data.) Figs. 1 and 3 show the phase of the sinusoidal temperature response of the coating at the front surface (air/coating interface) relative to the sinusoidal heating by a pump beam incident on the front surface. Figures 2 and 4 show the phase of the sinusoidal temperature response of the coating at the rear surface (coating/substrate interface) relative to the sinusoidal heating by a pump beam incident on the front surface. The behavior is plotted as a function of the modulation frequency in all figures (In Figs. 3 and 4, x is proportional to the square root of the modulation frequency). Three curves are shown in Figs. 3 and 4. They correspond to different relative thermal effusivities of the coating and substrate. The g = 10 curves correspond to a thermally insulating coating on a thermally conductive substrate. The g = 0.1 curves correspond to a thermally conductive coating on a thermally insulating substrate. The g=1 curves correspond to thermally matched coating and substrate. The plotted case of

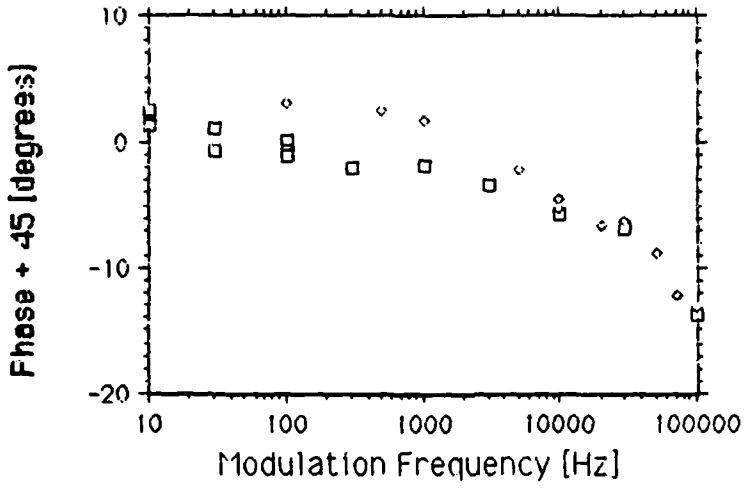

Fig. 1 Front-Surface Phase vs Modulation Frequency

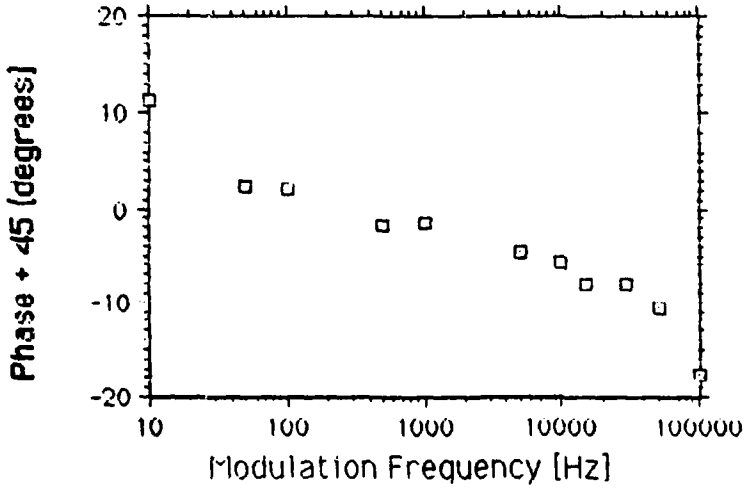

Fig. 2 Rear-Surface Phase vs Modulation Frequency

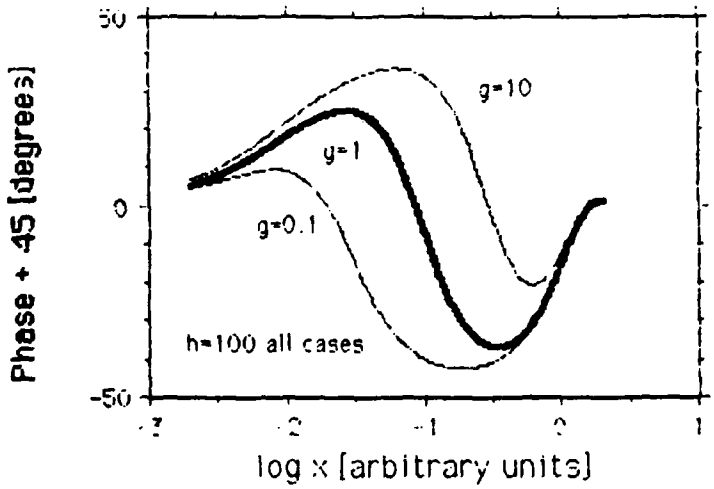

Fig. 3 Front Surface Phase vs Log Sqrt Modulation Freq

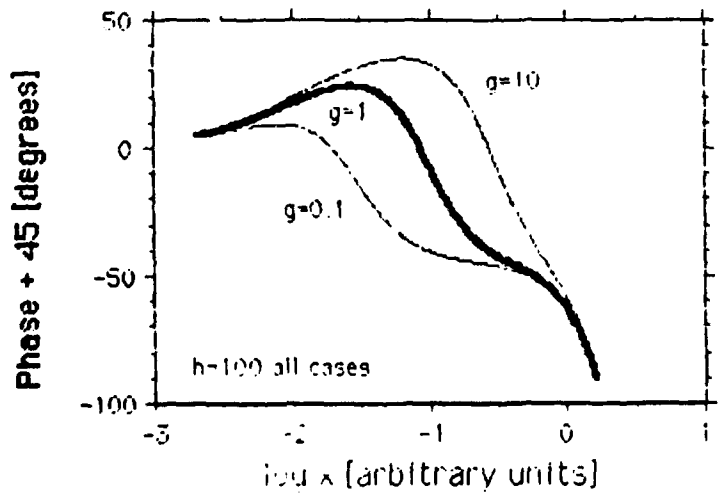

Fig.4 Rear Surface Phase vs Log Sqrt Modulation Freq

h = 100 corresponds to a relatively large thermal contact resistance.

2.4.2 Detailed Theoretical Behavior

In Figs. 3 and 4 the oscillations are the result of interference between the direct heating, and the diffusion waves that are partially reflected at interfaces. The interference oscillations in Fig. 3 are confined to the range $-45^{o} < \phi < 45^{o}$ where ϕ is phase. The oscillations decrease exponentially in amplitude for arguments greater than those plotted because of the critically damped nature of diffusion waves. The lowest frequency zero crossing shown is present only for non-negligible values of the thermal contact resistance between the coating and the substrate. The phase in Fig. 4 decreases monotonically for arguments greater than those plotted because of the finite transit time for thermal waves to propagate through the coating. (The diffusion waves are generated at the front surface but detected at the rear surface in this case.)

2.4.3 Discussion of Experimental Data

The zero crossings in both figures imply the presence of a non-negligible contact resistance. The two data sets plotted in Fig. 1 were measured about one week apart at approximately the same point on the sample. The source of the nonreproducibility of the low-frequency data is not known; additional studies are in progress to provide an explanation. Although a three-parameter

model has been derived to fit the data, a three-parameter fitting routine has not been implemented yet. This joining of theory and experiment is the next major milestone to be met. At the present stage, the experimental data appear to be consistent with the derived model behavior (within the general trends that can be identified without knowing the values of the fitting parameters corresponding to the experimental data).

2.5 THEORETICAL MODELLING

2.5.1 Background

One of the goals of this research is to characterize the thermal transport properties of dielectric coatings. In order that the thermal diffusion wave be generated in a layer thin compared to the coating thickness, it is necessary to deposit a thin metal layer over a dielctric coating under study. The presence of a second coating layer introduces additional interference structure into the data, which must be modelled. An analytic boundary value solution to the thermal diffusion equation has been obtained under the following assumptions: two coating layers, sinusoidal heating, one-dimensional heat flow normal to the surface, piecewise constant approximation, neglect of the effect of nonzero optical depth of the pump laser beam, infinite substrate thickness and thermally thin interfaces of nonnegligible thermal contact resistance. The approach is a generalization of that described in Ref. 6.

2.5.2 Analysis

2.5.2.1 Boundary Value Equation

The temperature and heat flux at the surface may be related to the temperature and heat flux at the substrate by the following equation (Ref. 6.8).

$$\begin{pmatrix} T \\ f \end{pmatrix}_{surface} = \begin{pmatrix} C_1 & S_1/\xi_1 \\ \xi_1 S_1 & C_1 \end{pmatrix} \begin{pmatrix} 1 & R_{12} \\ 0 & 1 \end{pmatrix} \begin{pmatrix} C_2 & S_2/\xi_2 \\ \xi_2 S_2 & C_2 \end{pmatrix} \begin{pmatrix} 1 & R_{23} \\ 0 & 1 \end{pmatrix} \begin{pmatrix} T \\ f \end{pmatrix}_{substrate} \quad (1)$$

where T = temperature

f = heat flux

$= -K \nabla T$

where K_j = thermal conductivity of layer j

$\xi_j = K_j k_j (1+i)$

where $i = \sqrt{-1}$

k_j = thermal diffusion-wave number

$= (\pi f / \kappa_j)^{1/2}$

where f = modulation frequency

κ_j = thermal diffusivity of layer j

and where $C_j = \cosh k_j \ell_j (1+i)$

$S_j = \sinh k_j \ell_j (1+i)$

where ℓ_j = thickness of layer j

and where R_{ij} = thermal contact resistance of unit area between regions i and j.

Subscripts 1, 2, and 3 refer to the outer coating layer (metal), the intermediate coating layer, and the substrate respectively. This model can be used to describe two cases: either that of a dielectric layer with a metal overcoat, and thermally thin interfaces between the layers, or that of a metal coating with a thermally thick interface to the substrate.

2.5.2.2 Boundary Value Solution

Equation (1) was solved to obtain the temperature at the surface in terms of the flux at the surface, noting that the substrate is assumed to be infinitely thick, and so the solution in the substrate contains no terms propagating toward the surface. The solution is:

$$T_{surface} = \frac{f_{surface}}{\xi_1}\left(\frac{A_{cc}C_1C_2+A_{cs}C_1S_2+A_{sc}S_1C_2+A_{ss}S_1S_2}{B_{cc}C_1C_2+B_{cs}C_1S_2+B_{sc}S_1C_2+B_{ss}S_1S_2}\right) \qquad (2)$$

where

$$A_{cc} = \alpha_1 + i\beta_1$$
$$A_{cs} = \alpha_2 + i\beta_2$$
$$A_{sc} = \alpha_3 + i\beta_3$$
$$A_{ss} = \alpha_4 + i\beta_4$$

and

$$B_{cc} = A_{sc}$$

$$B_{cs} = A_{ss}$$

$$B_{sc} = A_{cc}$$

$$B_{ss} = A_{cs}$$

and where

$$\alpha_1 = 1 + h_{23}x_2/\sqrt{\pi} + g_{23}h_{12}x_1/\sqrt{\pi}$$

$$\beta_1 = h_{23}x_2/\sqrt{\pi} + g_{23}h_{12}x_1/\sqrt{\pi}$$

$$\alpha_2 = h_{12}x_1/\sqrt{\pi} + g_{23}$$

$$\beta_2 = h_{12}x_1/\sqrt{\pi} + 2h_{12}x_1\ h_{23}x_2/\pi$$

$$\alpha_3 = g_{23}\ g_{12}$$

$$\beta_3 = 0$$

$$\alpha_4 = g_{12} + g_{12}\ h_{23}x_2/\sqrt{\pi}$$

$$\beta_4 = g_{12}\ h_{23}x_2/\sqrt{\pi}\ .$$

In these equations x_j, g_{ij} and h_{ij} are dimensionless parameters defined as follows:

$$x_1 = (\pi f/f_{c,1})^{1/2}$$

$$x_2 = (\pi f/f_{c,2})^{1/2}$$

where

$$f_{c,1} = \kappa_1 / \ell_1^2$$

$$f_{c,2} = \kappa_2 / \ell_2^2$$

$f_{c,j}$ are characteristic frequencies above which thermal diffusion wave interference effects are absent, due to the critically damped nature of oscillatory solutions to the diffusion equation.

The modulation frequency f is the independent variable in the problem.

$$g_{12} = \xi_2 / \xi_1$$

$$g_{23} = \xi_3 / \xi_2$$

g_{ij} are ratios of effusivities of the respective layers (Ref. 9). When $g_{ij} = 1$, then the regions i and j are thermally matched, and there is no reflection of the thermal diffusion wave at the interface. Thus, the ratio of effusivities is to thermal diffusion waves at an interface what the ratio of refractive indices is to light waves at an interface.

$$h_{12} = R_{12} / R_{2,c}$$

$$h_{23} = R_{23} / R_{3,c}$$

where

$$R_{2,c} = 1 / e_2 \sqrt{\pi f_{c,1}}$$

$$R_{3,c} = 1 / e_3 \sqrt{\pi f_{c,2}}$$

where

$$e_j = K_j / \sqrt{\kappa}_j$$

Here, e_j is the thermal effusivity of region j, and $R_{j,c}$ is characteristic thermal resistance of region j, for a layer in region j whose thickness is defined by the characteristic frequency of layer j-1, (Ref. 6), $h_{i,j}$ is a dimensionless parameter proportional to the contact resistance between regions i and j, but also with implicit dependences indicated by the definitions.

In equation (2), the time-independent complex phase of the heat flux at the surface is zero, and the time-independent

complex phase of the temperature at the surface is the phase shift between the heating and the temperature response. This phase is to be equated to the phase measured in the experiment by the lock-in analyzer as a function of modulation frequency f.

2.5.2.3 Complex Phase of Solution

If the complex components of Eq. (2) are separated, then the complex phase is given by:

$$\phi = \phi_{\text{numerator}}{}^{k} - \phi_{\text{denominator}} - \pi/4 \qquad (3)$$

where numerator and denominator refer to the fraction within the parentheses, and the $\pi/4$ is due to the divisor ξ_1. In this equation,

$$\phi_{\text{numerator}} = \tan^{-1}\left[\frac{\text{Im(numerator)}}{\text{Re(numerator)}}\right]$$

$$\phi_{\text{denominator}} = \tan^{-1}\left[\frac{\text{Im(denominator)}}{\text{Re(denominator)}}\right]$$

where

$$\begin{aligned}
\text{Re(numerator)} &= \alpha_1(cc_1cc_2 - ss_1ss_2) - \beta_1(ss_1cc_2 + cc_1ss_2) \\
&+ \alpha_2(cc_1sc_2 - ss_1cs_2) - \beta_2(ss_1sc_2 + cc_1cs_2) \\
&+ \alpha_3(sc_1cc_2 - cs_1ss_2) - \beta_3(cs_1cc_2 + sc_1ss_2) \\
&+ \alpha_4(sc_1sc_2 - cs_1cs_2) - \beta_4(cs_1sc_2 + sc_1cs_2) \\
\text{Im(numerator)} &= \alpha_1(ss_1cc_2 + cc_1ss_2) + \beta_1(cc_1cc_2 - ss_1ss_2) \\
&+ \alpha_2(ss_1sc_2 + cc_1cs_2) + \beta_2(cc_1sc_2 - ss_1cs_2) \\
&+ \alpha_3(cs_1cc_2 + sc_1ss_2) + \beta_3(sc_1cc_2 - cs_1ss_2) \\
&+ \alpha_4(cs_1sc_2 + sc_1cs_2) + \beta_4(sc_1sc_2 - cs_1cs_2)
\end{aligned}$$

and where the corresponding real and imaginary parts of the denominator are obtained by letting

$$1 \rightarrow 3$$

$$2 \rightarrow 4$$

$$3 \rightarrow 1$$

$$4 \rightarrow 2$$

in the and coefficient subscripts. In these expressions,

$$cc_j = \cosh(x_j)\cos(x_j)$$

$$cs_j = \cosh(x_j)\sin(x_j)$$

$$sc_j = \sinh(x_j)\cos(x_j)$$

$$ss_j = \sinh(x_j)\sin(x_j)$$

2.5.3 Graphical Presentation of Theoretical Solution

The theoretical expression for phase Eq. (3) contains six adjustable parameters (g_{12}, g_{23}, h_{12}, h_{23}, $f_{c,1}$, $f_{c,2}$) and one independent variable f. The full complexity of the solution behavior has not been explored yet. One illustrative example is presented here. Figure 5 shows interference oscillations in the phase for a high contrast case consisting of two coatings of high thermal conductivity deposited on a substrate of high thermal conductivity, and with interfaces of low thermal conductivity between the coatings. The alternation of high and low conductivities is responsible for the high contrast of the interference oscillations. Points to be noted include the

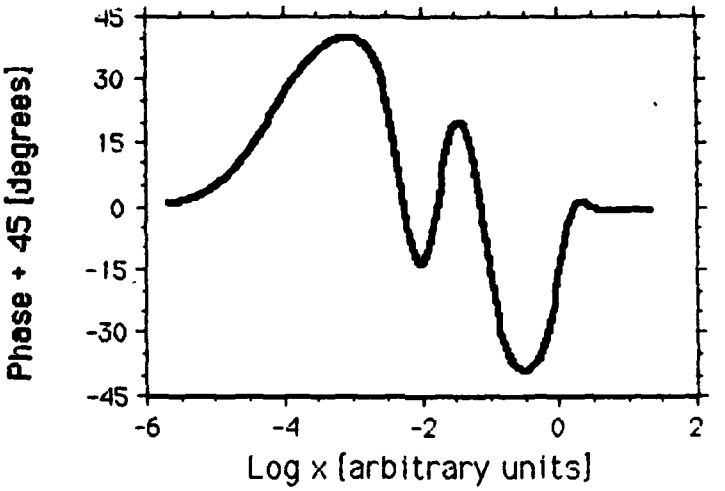

Fig 5 Two-Layer Coating (High Contrast Case)

following. The oscillations damp out at high modulation frequencies due to the critically damped nature of thermal diffusion waves. The frequencies and phases at the four principal phase extrema constitute theoretical data structure to be matched to measured data. Note that these features span six decades of modulation frequencies. The present measurement apparatus will tune over only four decades (10 Hz to 100 kHz). If the rear surface probe can be applied to two-layer coatings without the introduction of systematic errors (which remains to be seen), then the equivalent of at least one independent feature can be obtained without the need for additional dynamic range in modulation frequency. This example again illustrates the necessity of developing the greatest possible system dynamic range in order to capture data over a sufficient interval of interference oscillations to assure uniqueness in fitting the adjustable parameters.

3.0 CONCLUSION

An improved measurement system for performing thermal transport studies in coatings, interfaces, and surfaces has been developed and implemented. A major source of systematic error in earlier work has been discovered and eliminated. Measured data are in qualitative agreement with theoretically predicted behavior; numerical fitting of the data constitutes the next research phase. Efforts continue to characterize in detail

thermal transport in simple, thin layered structures. Initial theoretical modelling of more complicated two-layer structures is reported.

4.0 REFERENCES

[1] Lange, M.R., McIver, J.K., Guenther, A.H., and Walker, T.W. Nat. Bur. Stand. (U.S.) Spec. Publ. 669, 380-386 (1984)

[2] Decker, D.L., Kashigoe, L.G., and Ashley, E.J., Nat. Bur. Stand. (U.S.) Spec. Publ. 727, 291-297 (1986).

[3] Akhtar, S.M.J., Ristau, D., and Ebert J., Nat. Bur. Stand. (U.S.) Spec. Publ. 752, 345-351 (1986).

[4] Jacobs, S., LLE Review Quarterly Report 29, 30-38 (1986).

[5] Swimm, R.T., Appl. Phys. Lett. 42, 955-957 (1983)

[6] Swimm, R.T., and Hou, L., Nat. Bur. Stand. (U.S.) Spec. Publ. 752, 251-258 (1986).

[7] Swimm, R.T., Proc. 1987 Boulder Damage Symposium, to be published in a Nat. Bur. Stand. (U.S.) Spec. Publ.